The Regulators of Peroxisomal Acyl-Carnitine Shuttle CROT and CRAT Promote Metastasis in Melanoma

JID Open

Irene Lasheras-Otero[1,2], Iker Feliu[2,3], Alberto Maillo[4], Haritz Moreno[2,3], Marta Redondo-Muñoz[1,2], Paula Aldaz[1,2], Ana Bocanegra[5], Ana Olias-Arjona[1,2], Fernando Lecanda[2,3,6,7], Joaquin Fernandez-Irigoyen[2,8], Enrique Santamaria[2,9], Ignacio M. Larrayoz[10,11], David Gomez-Cabrero[2,4,12], Claudia Wellbrock[1], Silvestre Vicent[2,3,6,13] and Imanol Arozarena[1,2,13]

Circulating tumor cells are the key link between a primary tumor and distant metastases, but once in the bloodstream, loss of adhesion induces cell death. To identify the mechanisms relevant for melanoma circulating tumor cell survival, we performed RNA sequencing and discovered that detached melanoma cells and isolated melanoma circulating tumor cells rewire lipid metabolism by upregulating fatty acid (FA) transport and FA beta-oxidation–related genes. In patients with melanoma, high expression of FA transporters and FA beta-oxidation enzymes significantly correlates with reduced progression-free and overall survival. Among the highest expressed regulators in melanoma circulating tumor cells were the carnitine transferases carnitine O-octanoyltransferase and carnitine acetyltransferase, which control the shuttle of peroxisome-derived medium-chain FAs toward mitochondria to fuel mitochondrial FA beta-oxidation. Knockdown of carnitine O-octanoyltransferase or carnitine acetyltransferase and short-term treatment with peroxisomal or mitochondrial FA beta-oxidation inhibitors thioridazine or ranolazine suppressed melanoma metastasis in mice. Carnitine O-octanoyltransferase and carnitine acetyltransferase depletion could be rescued by medium-chain FA supplementation, indicating that the peroxisomal supply of FAs is crucial for the survival of nonadherent melanoma cells. Our study identifies targeting the FA-based cross-talk between peroxisomes and mitochondria as a potential therapeutic opportunity to challenge melanoma progression. Moreover, the discovery of the antimetastatic activity of the Food and Drug Administration–approved drug ranolazine carries translational potential.

Journal of Investigative Dermatology (2023) **143,** 305–316; doi:10.1016/j.jid.2022.08.038

[1]*Cancer Signaling Unit, Navarrabiomed, University Hospital of Navarra (HUN), Public University of Navarra (UPNA), Pamplona, Spain;* [2]*IdiSNA, Navarra Institute for Health Research, Pamplona, Spain;* [3]*Program in Solid Tumors, Centre for Applied Medical Research, University of Navarra, Pamplona, Spain;* [4]*Translational Bioinformatics Unit, Navarrabiomed, University Hospital of Navarra (HUN), Public University of Navarra (UPNA), Pamplona, Spain;* [5]*Oncoimmunology Group, Navarrabiomed, Navarrabiomed, University Hospital of Navarra (HUN), Public University of Navarra (UPNA), Pamplona, Spain;* [6]*Center for Biomedical Research Network on Cancer (CIBERONC), Madrid, Spain;* [7]*Department of Pathology, Anatomy and Physiology, School of Medicine, University of Navarra, Pamplona, Spain;* [8]*Proteomics Platform, Navarrabiomed, University Hospital of Navarra (HUN), Public University of Navarra (UPNA), Pamplona, Spain;* [9]*Clinical Neuroproteomics Unit, Navarrabiomed, University Hospital of Navarra (HUN), Public University of Navarra (UPNA), Pamplona, Spain;* [10]*Biomarkers and Molecular Signaling Group, Center for Biomedical Research of La Rioja (CIBIR), Foundation Rioja Salud, Logroño, Spain;* [11]*Pre-departmental Nursing Unit, University of La Rioja (UR), Logroño, La Rioja, Spain; and* [12]*Biological and Environmental Sciences and Engineering Division, King Abdullah University of Science and Technology, Thuwal, Saudi Arabia*

[13]*These authors contributed equally as senior authors.*

Correspondence: Imanol Arozarena, Cancer Signaling Unit, Navarrabiomed, University Hospital of Navarra (HUN), Public University of Navarra (UPNA), 31008 Pamplona, Spain. E-mail: iarozarm@navarra.es

Abbreviations: CRAT, carnitine acetyltransferase; CROT, carnitine O-octanoyltransferase; CTC, circulating tumor cell; FA, fatty acid; FAO, fatty acid beta-oxidation; MCFA, medium-chain fatty acid; siRNA, small interfering RNA

Received 11 May 2022; revised 26 July 2022; accepted 3 August 2022; accepted manuscript published online 1 September 2022; corrected proof published online 29 October 2022

INTRODUCTION

Cutaneous melanoma is responsible for over 80% of skin cancer–related deaths, but BRAF/mitogen-activated protein kinase kinase inhibitor combinations and immunotherapies have resulted in significant improvements (Luke et al., 2017; Wolchok et al., 2017). Nevertheless, the development of resistance mechanisms represents a major challenge (Trojaniello et al., 2021).

Melanoma tumors are considerably heterogeneous and frequently consist of populations of cells with distinct transcriptional states (Hoek et al., 2006; Tsoi et al., 2018) called melanoma phenotypes. Importantly, individual phenotypes ranging from an undifferentiated to a fully differentiated state can impact therapy (Arozarena and Wellbrock, 2019; Konieczkowski et al., 2014; Müller et al., 2014; Smith et al., 2017, 2013) and melanoma invasion and metastasis (Campbell et al., 2021; Chapman et al., 2014; Rowling et al., 2020). Crucially, heterogeneity in phenotype markers is also found in circulating tumor cells (CTCs) from patients with melanoma (Khoja et al., 2014).

CTCs are the key link between the primary tumor and distant metastases, and the adaptation of CTCs to the bloodstream environment may provide therapeutic opportunities to target metastasis. However, owing to the challenges associated with their isolation and long-term maintenance, information on CTCs functional properties remains limited.

Earlier studies have shown that CTCs slow down cell cycle progression and switch to an epithelial–mesenchymal transition transcriptional state (Micalizzi et al., 2017; Polioudaki et al., 2015). Nevertheless, above all, CTCs are exposed to nonadherent conditions in the blood, and to survive, they must overcome anoikis. Although the loss of integrin signaling and activation of death receptor signaling clearly play a part in the induction of anoikis (Simpson et al., 2008), detachment-associated cell death has also been linked to increased ROS production and cancer cells rewire metabolic activities to overcome this threat (Buchheit et al., 2014; Schafer et al., 2009). Melanoma CTCs were found to activate a distinct antiferroptosis program to reduce ROS (Hong et al., 2021). Nevertheless, this was only seen in a particular CTC population, whereas other CTC populations did not activate this program (Hong et al., 2021). This finding is entirely in line with the heterogeneity detectable in melanoma CTC populations from patients (Khoja et al., 2014) and implies that the means CTCs deploy to survive in the circulation are variable. Thus, if we are to target the vulnerabilities of melanoma CTCs to tackle metastatic disease, we need to gain a better understanding of the mechanisms that enable melanoma cells to propagate under nonadherent conditions.

RESULTS

Nonadherent melanoma cells display cell-autonomous characteristics of CTCs

We analyzed melanoma cells cultured in suspension in standard high glucose (25 mM) medium and, considering the average physiological blood glucose concentration (90–110 mg/dl), also in the presence of 5 mM (90 mg/dl) glucose. In addition, we included different melanoma cell phenotypes: differentiated 501mel (melanocytic phenotype) cells and undifferentiated WM266-4 (invasive phenotype) cells (Smith et al., 2017).

Detached melanoma cells were present as single cells or small cell clusters (shown are 501mel cells, Figure 1a) and exhibited an altered cell cycle progression (Figure 1b and Supplementary Figure S1a). In line with our previous findings (Ferguson et al., 2017), in adhered cells, glucose restriction to 5 mM decreased cell numbers in S-phase, with more cells present in G1, but this change was generally not seen in cells in suspension (Supplementary Figure S1a).

Over a period of 72 hours, 5–12% of cells in suspension were represented in the sub-G1 fraction (Figure 1c). Glucose restriction led to a slight increase in WM266-4 cells but had no significant impact on cell death in 501mel cells. After the initial induction of anoikis at 24–48 hours, no further increase in cell death occurred at 72 hours, suggesting that the cells were adapting to the suspension conditions.

Because we wanted to use suspension cells to identify the CTC functions relevant to metastasis, we tested the metastatic capacity of detached 501mel cells after tail-vein injection. Thirty minutes after injection (day 0), cells accumulated in the lungs (Figure 1d). After 7 days, although still noticeable throughout the mice, the cells had visibly homed to the liver (Figure 1d). Ex vivo analysis on day 28 revealed that the cells had colonized the liver and, to a lesser degree, the lungs (Figure 1e and f).

Principal component analysis after RNA sequencing of 501mel and WM266-4 cells showed that adhesion conditions affected cell identity more than glucose concentrations (Supplementary Figure S1b). This was also seen in both cell lines by hierarchical clustering analysis (Figure 1g and Supplementary Figure S1c). Genes upregulated in suspension were enriched in Gene Ontology terms linked to cell cycle arrest; autophagy, a process that can provide anoikis resistance (Fung et al., 2008); catabolic process; and fatty acid beta-oxidation (FAO) (Figure 1g). Genes downregulated in suspension were enriched for cholesterol biosynthetic process and lipid or acyl-CoA metabolic processes (Figure 1g). Similar results were found in WM266-4 cells (Supplementary Figure S1c).

Gene set enrichment analysis for cancer hallmarks identified epithelial–mesenchymal transition and coagulation enriched in 501mel suspension cells cultured in 5 or 25 mM glucose (Figure 1h and Supplementary Figure S1d), but most importantly, the same enrichment was seen in a dataset from CTCs (Figure 1i), which we had previously isolated from 501mel tumor-bearing mice (Rowling et al., 2020). Also, genes for TNFα– or IL-5–signal transducer and activator of transcription 5 signaling generally activated by cytokines in the blood were found enriched in 501mel CTCs (Figure 1i). This was however not seen in suspension cells (Figure 1h), suggesting that these rather activate cell-autonomous processes that might occur in CTCs.

Fatty acid transport and beta-oxidation are upregulated in 501mel CTCs and correlate with faster progression and poor patient survival

Gene Ontology enrichment analysis of detached 501mel cells showed that independent of glucose concentration, lack of adhesion induced a general rewiring of lipid metabolism. Suspension cells switched toward fatty acid (FA) catabolism, downregulating lipid biosynthetic processes but upregulating FAO (Figure 2a and b). The latter was reflected in the upregulation of genes involved in peroxisomal as well as mitochondrial FAO (Figure 2c). On the other hand, the key regulators of FA synthesis and storage such as stearoyl-CoA desaturase or FA synthase were downregulated (Figure 2c). Suspension cells also upregulated the intracellular FA transport machinery, including regulators of mitochondrial membrane (CPT1A, CPT1C, CPT2, and SLC25A20) and peroxisomal membrane transport (ABCD1, ABCD3) as well as carnitine O-octanoyltransferase (CROT) and carnitine acetyltransferase (CRAT), crucial regulators of FA shuttle between peroxisomes and mitochondria (Figure 2c). Similar results were obtained when analyzing the transcriptome of detached WM266-4 cells (Supplementary Figure S2a). Together this suggests that the upregulation of the FAO program is a direct response to a loss of adhesion, independent of melanoma phenotype and glucose availability.

Many of the genes whose expression was altered in suspension cells were also differentially expressed in 501mel CTCs, with *CPT1C*, *CROT*, *CRAT*, *SC25A20*, and *CPT2* among the highest expressed genes (Figure 2d). Comparable with suspension cells, there was an upregulation of FA transporter and FAO genes and a downregulation of FA synthesis regulators (Figure 2d).

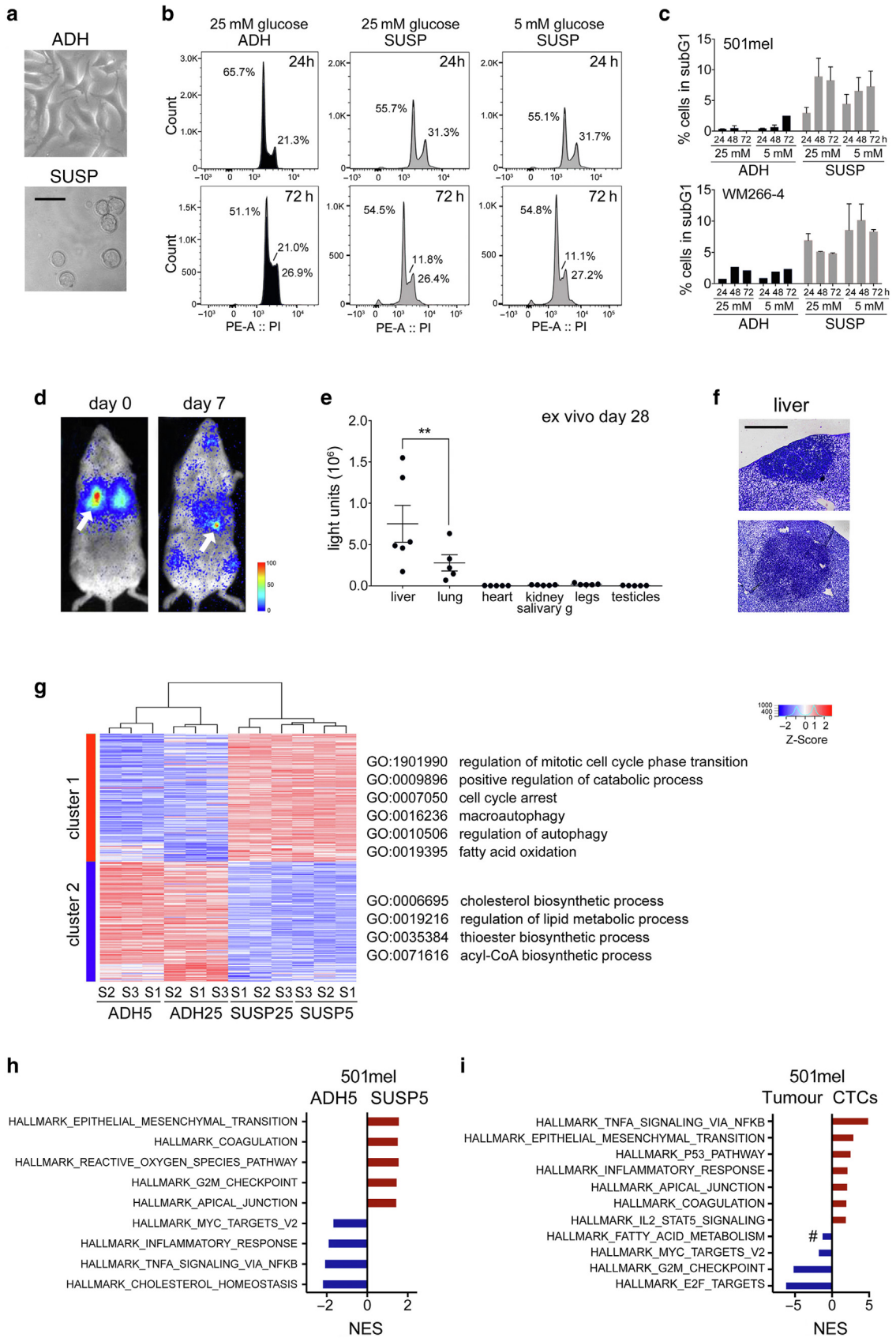

Figure 1. Cell-autonomous characteristics in nonadherent melanoma cells. (**a**) Representative image of 501mel cells in ADH or SUSP conditions. Bar = 50 μm. (**b**) Cell cycle profiles of 501mel cells cultured for 24 or 72 hours in ADH or SUSP condition in the presence of either 25 mM or 5 mM glucose. (**c**) Quantification of 501mel and WM266-4 cells detectable in sub-G1 over 72 hours. (**d**) Representative bioluminescent imaging of *Rag2/Ilgr2*$^{-/-}$ mice 30 min (day 0) or 7 days after injection with 501mel-GFP/luciferase cells, cultured in SUSP at 5 mM glucose. (**e**) Ex vivo bioluminescence quantification of 501mel tumor burden in

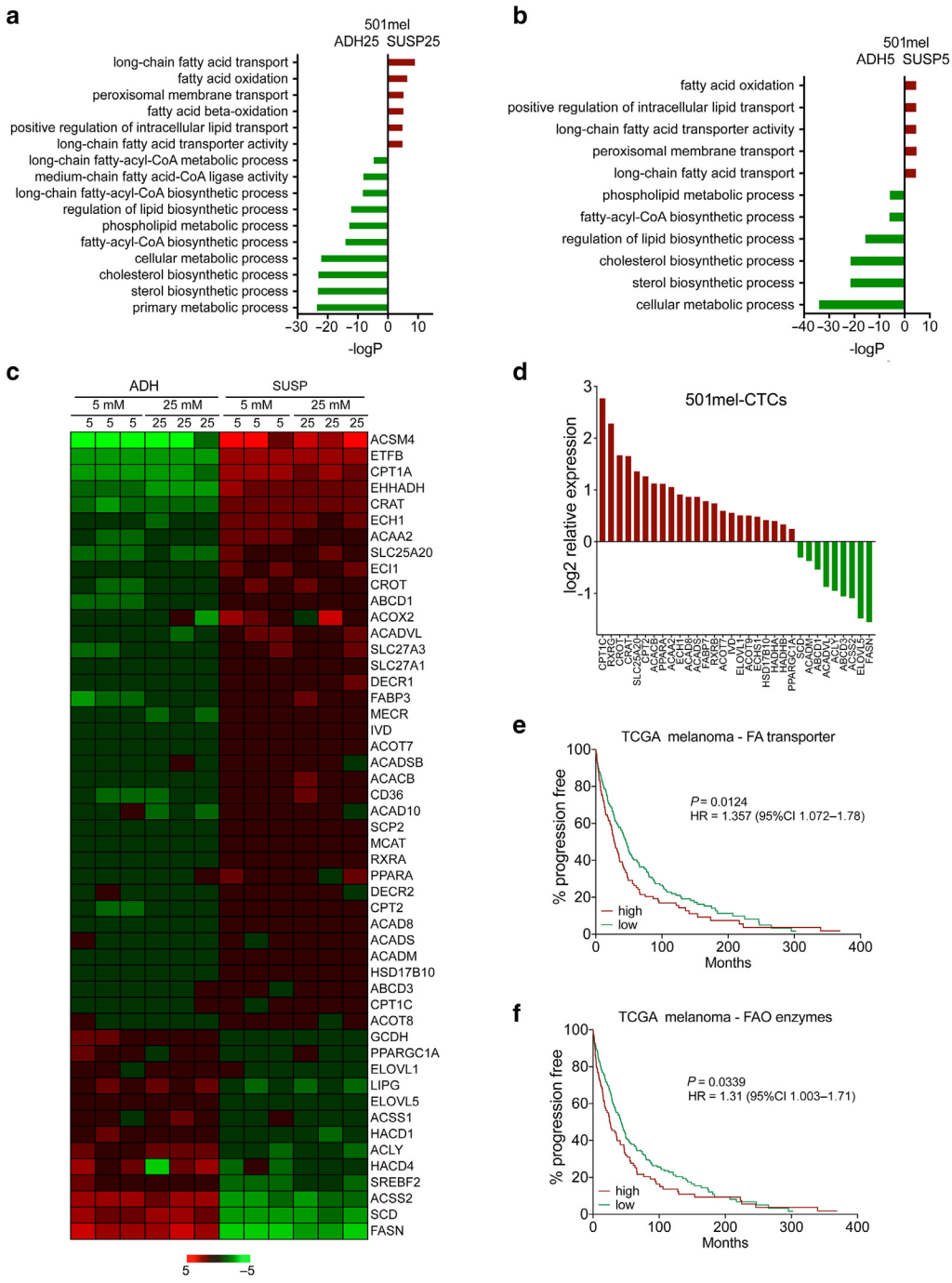

Figure 2. FAO regulators are upregulated in 501mel CTCs and correlate with faster disease progression. (**a, b**) Functional characteristics of 501mel suspension cells cultured in (**a**) 25 mM or (**b**) 5 mM glucose revealed by GSEA using GO term collections. (**c**) Heatmap of genes upregulated and downregulated in 501mel cells cultured in adhesion or suspension conditions in the presence of 5 or 25 mM glucose. (**d**) Genes related to FAO regulation upregulated and downregulated in 501mel CTCs. (**e**) Kaplan–Meier analysis of the TCGA melanoma patient cohort (Cancer Genome Atlas Network, 2015). Differences in progression-free survival for patients whose tumors express high or low levels of CPT1C, SLC25A20, CPT2, CPT1A, SLC27A1, SLC27A3, and CD36. Respective genes were analyzed for mRNA expression (z-score = 2.0) in cBioportal, and survival data were extracted and analyzed in GraphPad Prism. (**f**) Progression-free survival in the TCGA melanoma patient cohort for patients whose tumors express high or low levels of CROT, CRAT, ACACB, ACAA2, ECH1, ACADS, ACOT7, ACOT9, ECHS1, and HSD17B10. Respective genes were analyzed as described in **e**. ADH, adhesion; CI, confidence interval; con, control; CRAT, carnitine acetyltransferase; CROT, carnitine O-octanoyltransferase; CTC, circulating tumor cell; ERK2, extracellular signal–regulated kinase 2; FAO, fatty acid beta-oxidation; GO, Gene Ontology; GSEA, gene set enrichment analysis; HR, hazard ratio; siRNA, small interfering RNA; SUSP, suspension; TCGA, The Cancer Genome Atlas.

Interrogating The Cancer Genome Atlas melanoma database revealed that the expression of FA transporters and FAO enzymes upregulated in suspension cells and in 501mel CTCs significantly correlates with lower progression-free survival (median survival = 28.08 vs. 45.8 months and 25.18 vs. 42.41 months, respectively) and poorer survival (median survival = 66.7 vs. 111.1 months and 64.44 vs. 131.51 months, respectively) (Figure 2e and f and Supplementary Figure S2b and c).

different organs. Graphs show the mean ± SEM signal from six mice. (**f**) Representative images of H&E staining of liver metastases. Bar = 1,000 μm. (**g**) Hierarchical cluster analysis of differentially expressed genes ($P_{adj} < 0.001$) of 501mel cells cultured for 24 hours in ADH or SUSP (ADH vs. SUSP) in the presence of 25 or 5 mM glucose. (**h**) MSigDB hallmarks significantly (FDR < 0.05) enriched in 501mel cells cultured in SUSP or ADH in the presence of 5 mM glucose. (**i**) MSigDB hallmarks significantly (FDR < 0.05) enriched in either 501mel CTCs or 501mel subcutaneous tumors. Hash (#) denotes FDR = 0.076 for fatty acid metabolism. The 501mel CTCs had been isolated from 501mel tumor-bearing mice (Rowling et al., 2020). $^{**}P < 0.01$ with one-way ANOVA. ADH, adhesion; adj, adjusted; CTC, circulating tumor cell; FDR, false discovery rate; uh, hour; K, thousand; min, minute; MSigDB, Molecular Signatures Database; NES, normalized enrichment score; PE-A, phycoerythrin area; PI, propidium iodide; SUSP, suspension.

The carnitine transferases CROT and CRAT control anoikis in melanoma cells

To further corroborate our findings, we analyzed three additional melanoma cell lines: WM9 (melanocytic), WM98-1 (invasive), and MV3 (invasive). Independent of phenotype, CPT1A and CPT2 were significantly upregulated in suspension, whereas SLC25A20 expression was variable, and CPT1C was downregulated (Figure 3a). Apart from in WM266-4 cells, CROT and CRAT as well as the FAO enzymes EHHADH and TFB were also upregulated in suspension (Figure 3b). The upregulation of FAO transporters and enzymes was detectable at 24 hours (Figure 3a and b) and was still seen in cells cultured in suspension for 72 hours (Supplementary Figure S3a).

CROT, *CRAT*, and *SLC25A20* (also *CACT*) knockdown using small interfering RNA (siRNA) pools significantly reduced the capacity of 501mel cells to survive in suspension (Figure 3c). Using individual siRNAs, we confirmed that *CROT* or *CRAT* knockdown reduced the propagation of 501mel suspension cells (Figure 3d and Supplementary Figure S3b) but that the knockdown of *SLC25A20* had no significant effect (not shown). *CROT* or *CRAT* knockdown in adhered 501mel cells did not significantly impact cell number (Figure 3d), emphasizing the relevance of these carnitine transferases for the propagation of detached cells. Indeed, in suspension cells, *CROT* or *CRAT* knockdown over a period of 72 hours induced increased levels of cleaved caspase-3, but this was not seen in adhered cells (Figure 3e). A similar situation was observed with three other melanoma cell lines, where *CROT* or *CRAT* knockdown significantly reduced the propagation of cells in suspension, but again, no effect on cell number was seen in adhered cells (Figure 3f and g and Supplementary Figure S3c).

CROT and CRAT contribute to experimental metastasis of melanoma

We next assessed whether CROT and CRAT are playing a role in the metastatic process in vivo. Transient knockdown of *CROT* or *CRAT* in 501mel-luciferase cells injected into the tail-vein of immunodeficient mice (Figure 4a and Supplementary Figure S4a) resulted in a delay in metastasis (Figure 4b and c). On day 28, the whole-body signal of mice injected with *CRAT*-knockdown cells was significantly reduced (Figure 4b). A similar trend was observed in mice treated with CROT-targeted siRNA (Figure 4b and c), which did however not reach significance. The ex vivo analysis on day 28 of various organs revealed a reduction of light units in the livers of mice treated with CROT-targeted siRNA and CRAT-targeted siRNA, whereas signals in other organs apart from the lungs were considerably weaker (Supplementary Figure S4b). The signal reduction detectable in the liver (Figure 4d) remained significant when values were normalized to whole-body signals from the day of injection, whereas signals in the lungs did not reach significance (Figure 4e).

Clinical relevance for our findings is seen in The Cancer Genome Atlas melanoma cohort, where higher CRAT expression significantly correlates with progression within 2 years after diagnosis, and CROT and CRAT expression is significantly higher in patients surviving less than 2 years (Figure 4f and g and Supplementary Figure S4c–h).

Pharmacological inhibition of FAO suppresses the growth of nonadherent melanoma cells

CROT and *CRAT*, which were amongst the highest upregulated genes in 501mel CTCs (Figure 2d), are carnitine transferases (Houten et al., 2020) that play a central role in controlling the delivery of medium-chain FA (MCFA) from peroxisomes to mitochondria (Figure 5a). To assess whether the effect of *CROT* or *CRAT* knockdown on cell numbers is due to the limitation of MCFA, we depleted CROT or CRAT by RNA interference and determined suspension cell survival with or without supplementation of the MCFAs octanoyl acid or decanoyl acid. Both MCFAs could not only rescue the *CROT* or *CRAT* knockdown, but the addition of octanoyl acid and decanoyl acid even enhanced the propagation of suspension cells (Figure 5b), indicating metabolic rewiring in the absence of CROT or CRAT.

Our data suggest that regulating FA delivery of MCFA, derived from FAO in peroxisomes, is relevant for the survival of CTCs, possibly because MCFA fuels FAO in mitochondria. We therefore wished to further assess the relevance of FAO in peroxisomes and mitochondria for suspension cell survival. In the absence of specific CROT or CRAT inhibitors, we opted for two Food and Drug Administration–approved drugs (Figure 5a): thioridazine, which has been shown to target peroxisome-specific beta-oxidation (Leighton et al., 1984; Van den Branden and Roels, 1985), and ranolazine, which inhibits acetyl-CoA production from FAs in mitochondria (McCormack et al., 1998).

Reflecting the relevance of CROT and CRAT for peroxisome function, thioridazine very effectively suppressed 501mel cell propagation (Figure 5c). Supporting the importance of mitochondrial FAO, ranolazine also significantly decreased the growth of 501mel cells (Figure 5c). Importantly, we observed similar effects in five other melanoma cell lines (Figure 5d and e).

The pan-caspase inhibitor Z-VAD-FMK could effectively rescue the ranolazine-induced suppression of 501mel cell propagation, but this was much weaker for thioridazine (Figure 5f), implying additional mechanisms. Of note, FAO can also protect cells from ferroptosis because it consumes FAs and thus reduces the rate of lipid peroxidation. Indeed, two ferroptosis inhibitors, ferrostatin and liproxstatin, effectively increased cell propagation in the presence of thioridazine as well as ranolazine (Figure 5g). These data indicate that FAO is supporting the survival of detached melanoma cells, not only by suppressing apoptosis but also by limiting ferroptosis.

Inhibition of FAO impacts the metastatic spread of melanoma cells

We next assessed the role of FAO in organ colonization in vivo using 501mel cells. Before injection, suspension cells were pretreated in vitro with thioridazine or ranolazine, and the treatment continued in vivo for 7 days (Figure 6a) because 501mel cells had visibly homed to the liver during this time (Figure 1d). Whole-body luminescence analysis revealed that ranolazine and thioridazine significantly reduced tumor burden during the 7 days of treatment, and the effect was still

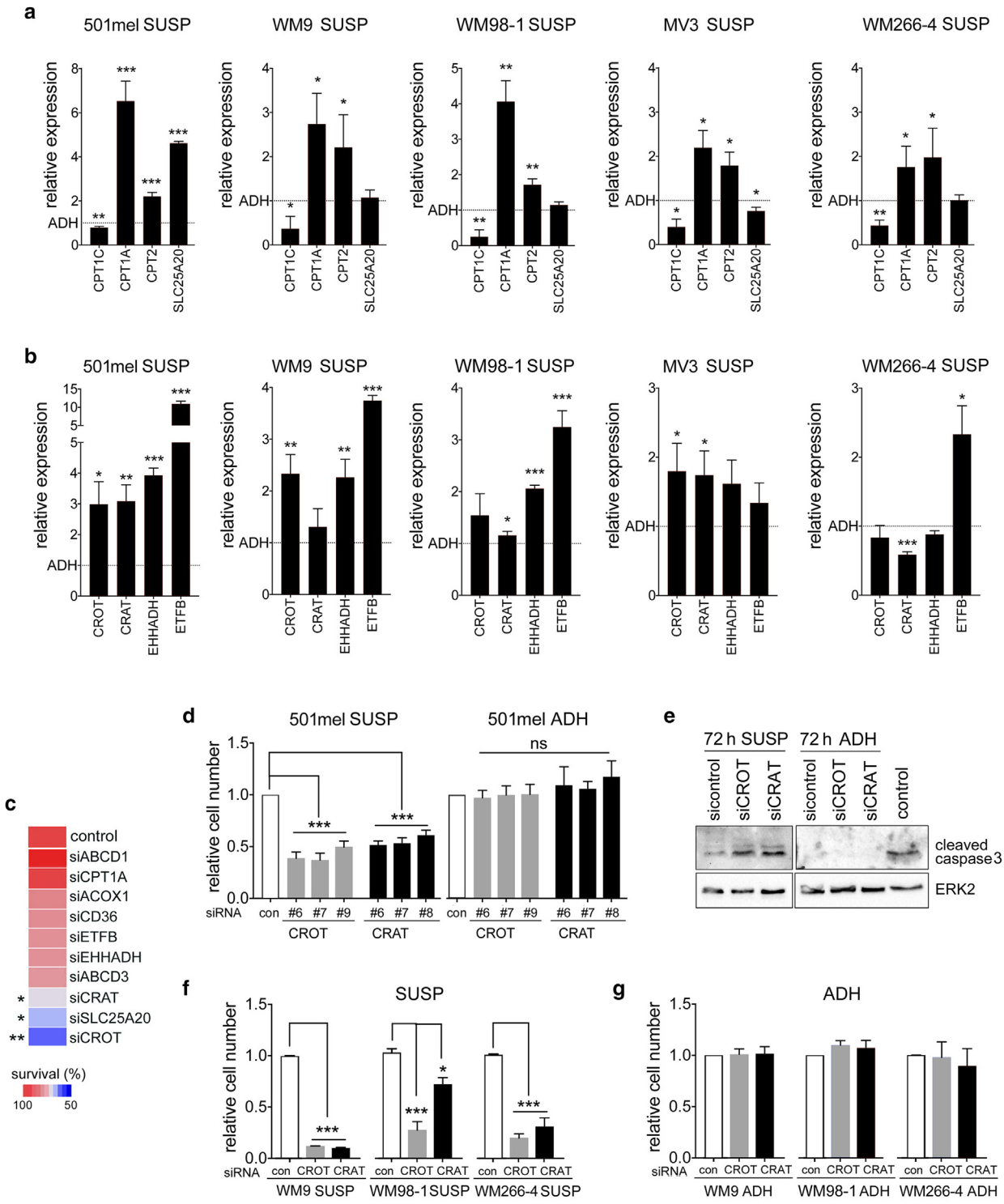

Figure 3. CROT and CRAT are required for the survival of nonadherent melanoma cells. (**a, b**) qPCR analysis of the indicated genes in the respective melanoma cells. Fold expression in cells grown in SUSP for 24 hours is indicated. The expression of cells grown in adhesion was set at 1. (**c**) Clonogenic survival analysis after replating 501mel cells grown for 72 hours in SUSP after a 48-hour knockdown of the indicated FAO regulators. Cells treated with control siRNA have been set at 100%. (**d**) Clonogenic survival analysis after replating 501mel cells grown in SUSP after knockdown of CROT or CRAT with three individual siRNAs. As a control, 501mel cells were cultured in adhesion conditions after the knockdown of CROT or CRAT with three individual siRNAs and quantified. Cells treated with control siRNA have been set 1. (**e**) Western blot for cleaved caspase-3 in 501mel cells treated with control-, CROT-, or CRAT-specific siRNA and cultured in SUSP or adhesion for 72 hours. Adherent cells treated with 1 μM staurosporine were used as cleaved caspase-3–positive control. ERK2 served as the loading control. (**f, g**) Analysis as in **d** in the indicated cell lines cultured in (**f**) SUSP or (**g**) adhesion using siRNA#6 for CRAT or CROT, respectively. Data show the mean ± SEM. $*P < 0.05$, $**P < 0.01$, and $***P < 0.001$ with one-way ANOVA and Student's *t*-test. ADH, adhesion; con, control; CRAT, carnitine acetyltransferase; CROT, carnitine O-octanoyltransferase; d, day; ERK2, extracellular signal–regulated kinase 2; FAO, fatty acid beta-oxidation; h, hour; ns, nonsignificant; siCRAT, carnitine acetyltransferase–targeted small interfering RNA; siCROT, carnitine O-octanoyltransferase–targeted small inmterfering RNA; siRNA, small interfering RNA; SUSP, suspension.

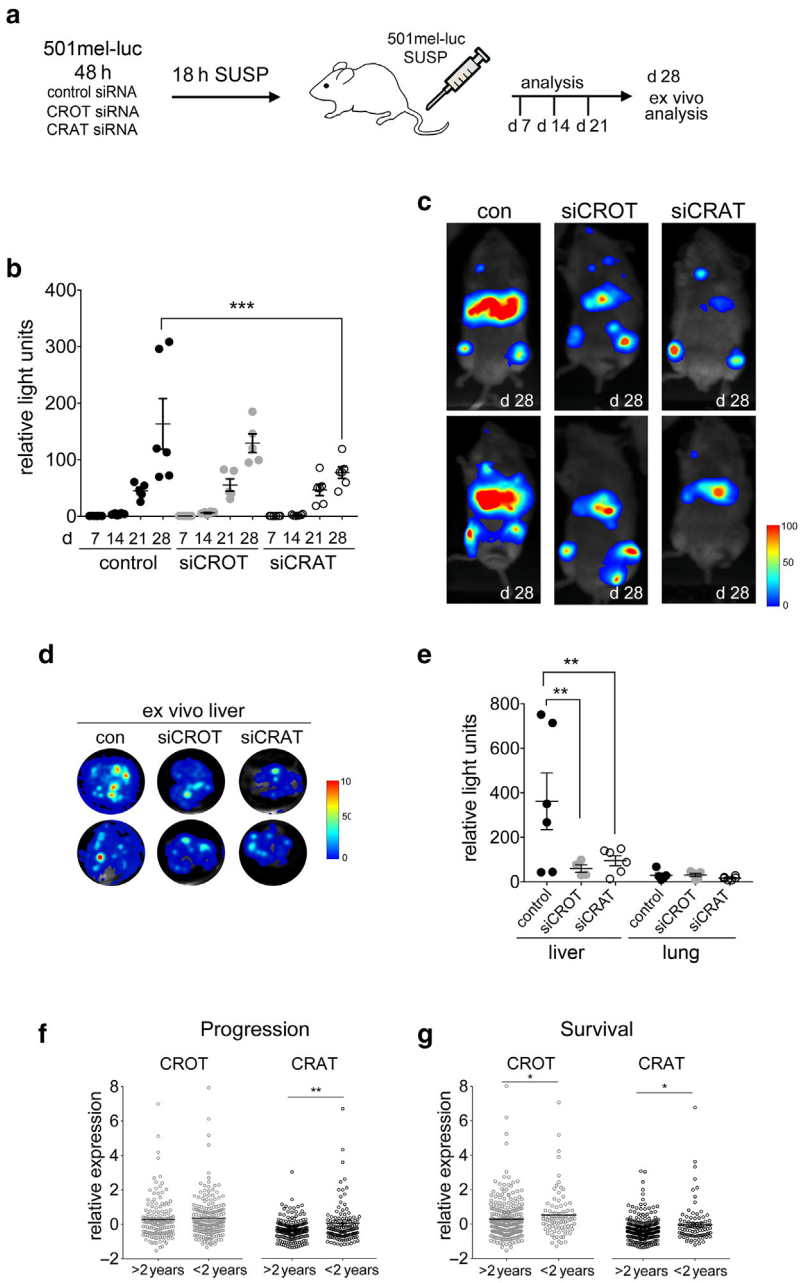

Figure 4. CROT and CRAT contribute to melanoma metastasis. (**a**) Experimental setup for the in vivo experiment. The 501mel cells were transfected with siRNA in adhesion (48 hours) and then cultured for 18 hours in SUSP before being counted and injected into the tail vein of *Rag2* mice. On days 7, 14, 21, and 28, whole-body bioluminescence imaging was performed. On day 28, mice were killed, and ex vivo bioluminescence imaging was performed on individual organs. (**b**) Full-body in vivo bioluminescence quantification of 501mel tumor burden over 28 days. Signals, normalized to day 0, from six (control, CRAT) or five (CROT) individual mice are shown. (**c**) Example images of full-body bioluminescence of control- or *Crot*- or *Crat*-knockdown mice on day 28. (**d**) Images of ex vivo bioluminescence in livers isolated from mice on day 28. (**e**) Ex vivo bioluminescence quantification of 501mel tumor burden in the indicated organs. Graphs show the signal of organs from six (control, CRAT) or five (CROT) mice. (**f, g**) Analysis of the TCGA melanoma patient cohort (Cancer Genome Atlas Network, 2015) for (**f**) progression-free or (**g**) overall survival in patients whose tumors express high or low levels of CROT or CRAT. $*P < 0.05$, $**P < 0.01$, and $***P < 0.001$ with one-way ANOVA and Student's *t*-test. con, control; CRAT, carnitine acetyltransferase; CROT, carnitine O-octanoyltransferase; d, day; luc, luciferase; siCRAT, carnitine acetyltransferase–targeted small interfering RNA; siCROT, carnitine O-octanoyltransferase–targeted small inmterfering RNA; siRNA, small interfering RNA; SUSP, suspension; TCGA, The Cancer Genome Atlas.

significant on day 14 (Figure 6b), indicating that the FAO inhibitors had impacted the initial establishment of metastasis. Nevertheless, after 21 days, although the trend of suppression was still visible, this did not reach significance (Figure 6b), suggesting that the effect of the drugs had worn off and that they did not produce inhibitory effects strong enough to be detectable in the whole mouse. After 28 days, mice were killed, and ex vivo analysis of liver and lung colonization was performed. Signals were strongest in the livers (Figure 6c), and although no significant change was detectable in the lungs, both ranolazine and thioridazine significantly reduced tumor load in the liver (Figure 6d).

DISCUSSION

Although the molecular mechanisms of melanoma migration and invasion have been studied in detail (Arozarena and Wellbrock, 2017; Ju et al., 2018), how melanoma cells survive under detached conditions during metastatic dissemination is less defined. We identified a functional link between FA catabolism, anoikis resistance, and metastatic potential of melanoma cells.

Similar to most CTCs (Tasdogan et al., 2021), melanoma CTCs exhibit elevated ROS levels compared with tumors, and antioxidants increase melanoma metastasis (Le Gal et al., 2015; Piskounova et al., 2015). Thus, the elimination of ROS appears crucial to succeed in metastasis, and a process that can reduce the insult of ROS is autophagy. Autophagy, which removes damaged mitochondria as the primary source of intracellular ROS, is known to counteract anoikis (Fung et al., 2008; Kongara and Karantza, 2012). Both 501mel and WM266-4 had significantly upregulated autophagy when cultured in suspension, which hence would enable

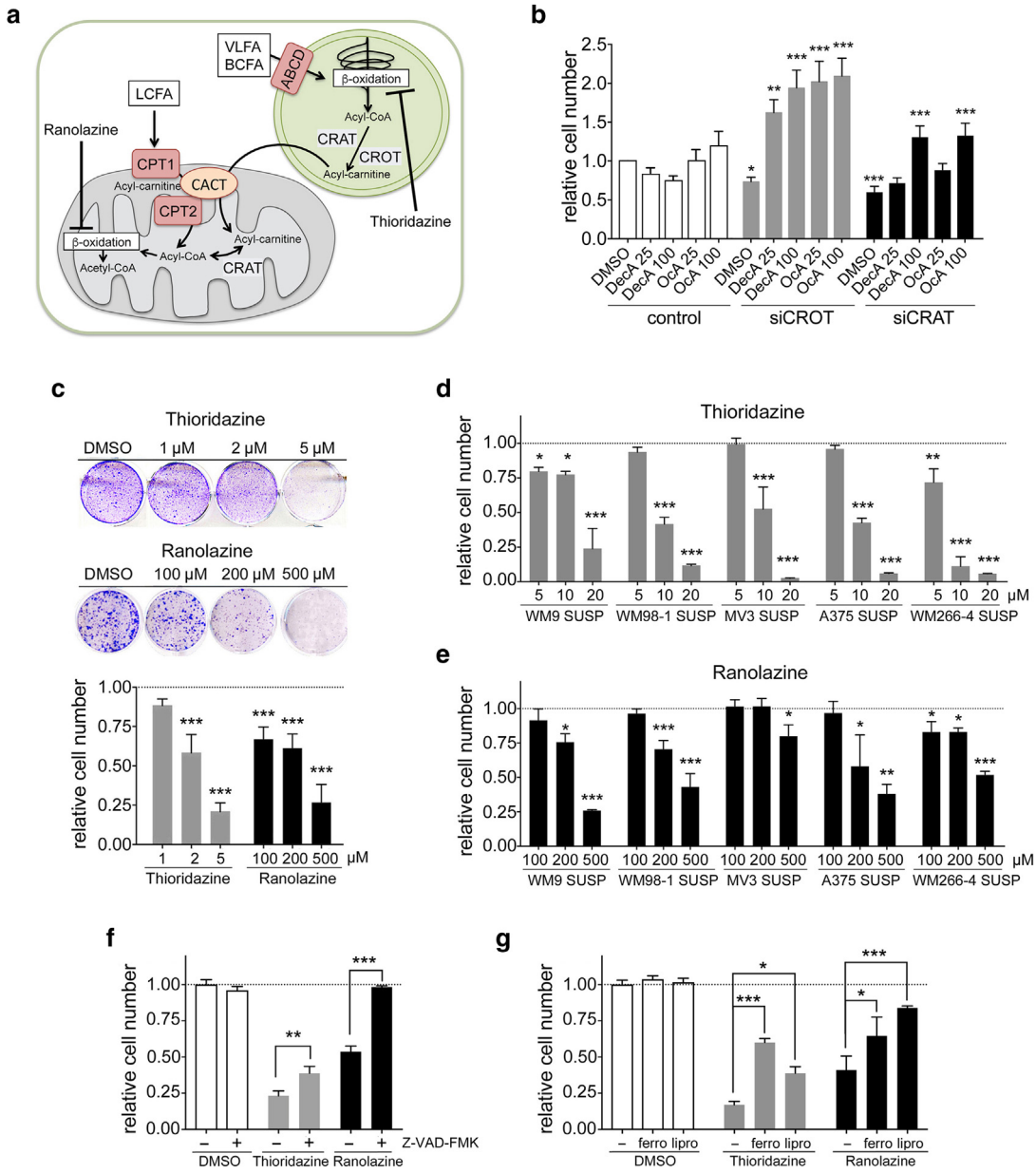

Figure 5. FAO inhibitors suppress the growth of nonadherent melanoma cells. (**a**) Schematic of FAO and acyl-carnitine shuttle. Peroxisomes catabolize VLFAs and BCFAs to MCFAs by beta-oxidation; the transport of these MCFA in form of acyl-carnitines to mitochondria is regulated by CROT and CRAT. In the absence of CROT or CRAT, the energy derived from VLFA and BCFA cannot be utilized. The action of FAO inhibitors is indicated. (**b**) Clonogenic survival analysis of 501mel cells grown for 72 hours in SUSP after knockdown of *Crot* or *Crat* in the presence or absence of the MCFAs OcA or DecA. Cells treated with control siRNA have been set 1. (**c**) Clonogenic survival analysis of 501mel cells grown for 72 hours in SUSP in the presence of the indicated FAO inhibitors. Control cells treated with DMSO have been set 1. Example images of the treated cells are shown. (**d, e**) Clonogenic survival analysis of the indicated cell lines grown for 72 hours in SUSP in the presence of (**d**) thioridazine or (**e**) ranolazine. (**f**) Clonogenic survival analysis of 501mel cells in the presence of the indicated FAO inhibitors and in the presence or absence of 50 μM Z-VAD-FMK. (**g**) Clonogenic survival analysis of 501mel cells in the presence of the indicated FAO inhibitors and in the presence or absence of either 1 μM ferro or 200 nM lipro. Data show the mean ± SEM. $*P < 0.05$, $**P < 0.01$, and $***P < 0.001$ with one-way ANOVA. BCFA, branched-chain fatty acid; CRAT, carnitine acetyltransferase; CROT, carnitine O-octanoyltransferase; DecA, decanoyl acid; FAO, fatty acid beta-oxidation; ferro, ferrostatin-1; LFA, long-chain fatty acid; lipro, liproxstatin-1; MCFA, medium-chain fatty acid; OcA, octanoyl acid; siCRAT, carnitine acetyltransferase–small interfering RNA; CROT, carnitine O-octanoyltransferase–small interfering RNA; siRNA, small interfering RNA; SUSP, suspension; VLFA, very-long-chain fatty acid.

them to modulate cellular ROS levels and contribute to survival.

Upregulation of autophagy can meet another important demand; during autophagy, engulfed damaged organelles are degraded, and this provides the cell with nutrients necessary for cell metabolism during cellular stress (Hernandez and Perera, 2022). Indeed, in leukemia cells, autophagy can regulate FA availability for FAO and consequently oxidative phosphorylation (Bosc et al., 2020). Importantly, activating FAO can also counteract excessive ROS because it produces the reducing equivalents nicotinamide adenine dinucleotide as well as flavin adenine dinucleotide.

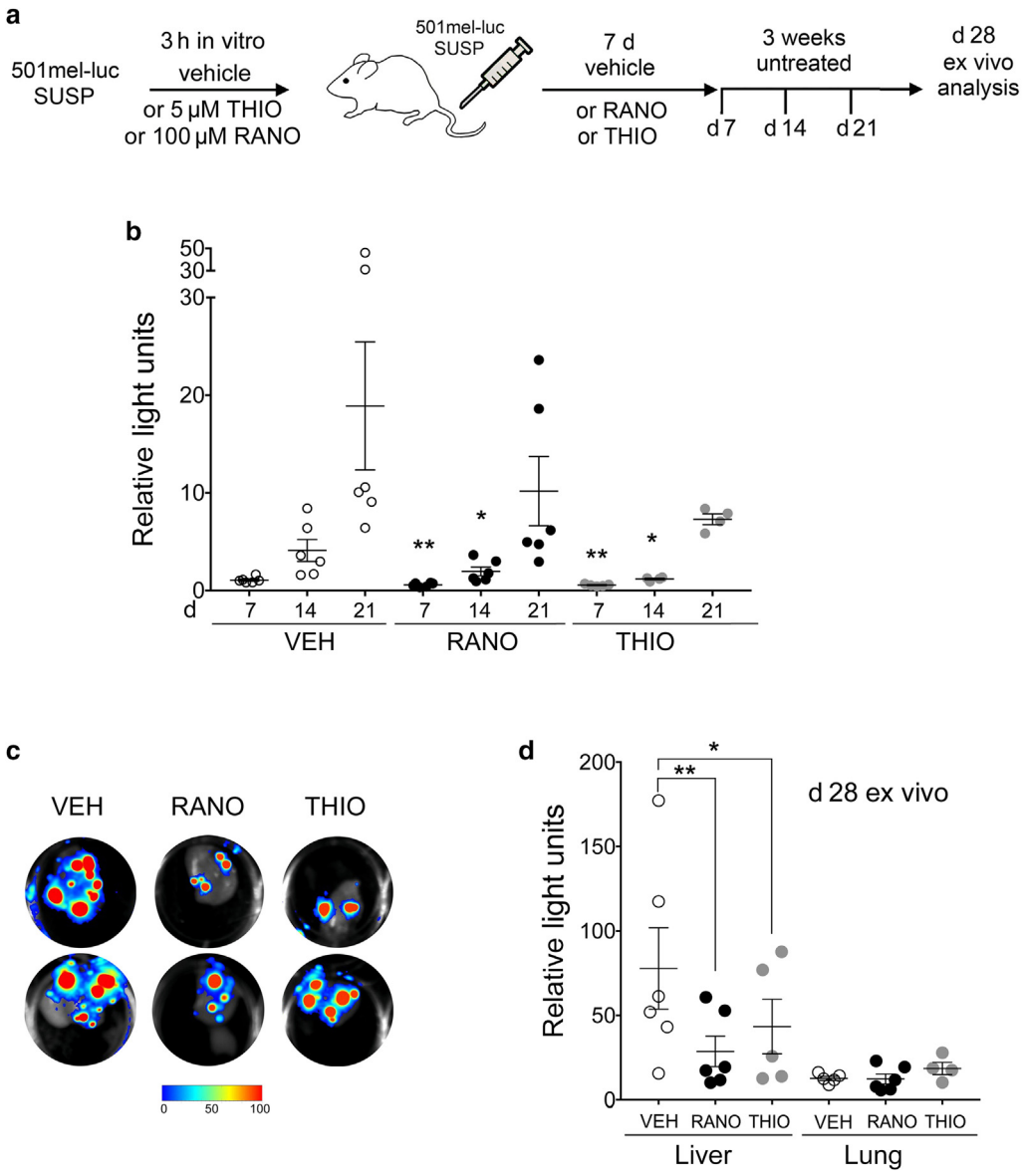

Figure 6. FAO inhibitors suppress melanoma metastasis. (**a**) Experimental setup for the in vivo experiment. Before injection suspension, cells were pretreated in vitro with a vehicle or 100 μM RANO or 5 μM THIO for 3 h. Treatment was continued in vivo with a vehicle, RANO (50 mg/kg/day), or THIO (10 mg/kg, every 2 days) for 7 days after injection, after which treatment was discontinued. On day 28, ex vivo analysis of individual organs was performed. (**b**) Full-body in vivo bioluminescence quantification of 501mel tumor burden over 21 days. Signals, normalized to day 0, from six (VEH control, RANO) or five (THIO) treated individual mice are shown. (**c**) Images of ex vivo bioluminescence in livers isolated from RANO-treated and THIO-treated mice on day 28. (**d**) Ex vivo bioluminescence quantification of 501mel tumor burden in the indicated organs. Graphs show the signal of organs from six (VEH control, RANO) or five (THIO) treated individual mice. $*P <$ 0.05 and $**P < 0.01$ with one-way ANOVA. d, day; FAO, fatty acid beta-oxidation; h, hour; luc, luciferase; RANO, ranolazine; THIO, thioridazine; VEH, vehicle.

FAO has been previously connected to anoikis and metastasis, with CPT1A as a key player, in a colorectal cancer model, in which blocking FAO led to ROS accumulation (Wang et al., 2018). Likewise, CD36 is a marker for metastasis-initiating cells that express higher levels of FAO enzymes, and a high-fat diet promotes CD36-positive initiated metastasis (Pascual et al., 2017). We found that CPT1A, CD36, and FAO enzymes were upregulated in detached melanoma cells, and intriguingly, this was independent of their phenotype with respect to differentiated melanocytic or undifferentiated invasive.

Some FA metabolism regulators have been linked to melanoma CTCs and their phenotype. For instance, PGC1α (*PPARGC1A*), which acts as a cofactor in the induction of FAO gene expression, is highly expressed in the melanocytic phenotype (Vazquez et al., 2013), and low PGC1α expression was detected in melanoma CTCs and correlated with increased metastasis (Luo et al., 2016). However, metastasis induced by PGC1α-low cells was linked to a mechanism independent of PGC1α's role in metabolism.

Single-cell analysis of CTCs isolated from patients with melanoma identified SREBP2 (*SREBF2*), the master regulator of cholesterol homeostasis, as an important factor in CTC survival, where it induced the expression of transferrin, which could counteract ROS-induced ferroptosis (Hong et al., 2021). Again, the mechanism of SREBP2-mediated CTC survival was not related to a particular metabolic state. Furthermore, the SREBP2 transcriptional program was predominantly expressed in a population of CTCs that shared characteristics with both the melanocytic and invasive phenotypes. Thus, the melanoma differentiation phenotypes might not accurately describe metabolic phenotypes in CTCs. This is in line with our findings that FAO upregulation did not correlate with a particular melanoma differentiation phenotype, and in fact, in both phenotypes, the strongest induced gene in detached cells was the same, medium-chain

acyl-CoA synthetase 4 (*ACSM4*). ACSM4 is a predicted mitochondrial medium-chain acyl-CoA synthetase (Watkins et al., 2007). ACSM activate free FAs to generate acyl-CoA, but the particular role of ACSM4 in FA metabolism is so far unknown. Potentially, ACSM4 could enable the activation of free FA released through lipophagy.

As mentioned earlier, FAO is required for metastasis (Pascual et al., 2017; Wang et al., 2018), and we find that thioridazine and ranolazine reduced the prometastatic activity of detached melanoma cells. Thioridazine, a first-generation antipsychotic drug, has other targets such as dopamine receptors and the KCNH2 potassium channel (Feinberg et al., 2022), but in melanoma, acting as an inhibitor of peroxisomal FAO (Leighton et al., 1984; Van den Branden and Roels, 1985), it could suppress BRAF inhibitor–induced drug tolerance (Shen et al., 2020). Ranolazine on the other hand inhibits acetyl-CoA production from FAs in mitochondria (McCormack et al., 1998).

The cross-talk between peroxisomes and mitochondria is controlled by the carnitine-shuttle enzymes CROT and CRAT, both of which are peroxisomal enzymes (Houten et al., 2020). Nevertheless, depending on alternative splicing, CRAT can also be expressed in mitochondria, and for instance, in skeletal muscle cells, mitochondrial CRAT can act as a distinct metabolic rheostat (Muoio et al., 2012; Seiler et al., 2014). However, it appears that in melanoma cells, CROT and CRAT assume very similar and closely linked functions in FA metabolism–controlled survival because we observed that cell death induced by either carnitine transferase could be rescued by MCFAs. Moreover, a double knockdown of *CROT* and *CRAT* did not increase the impact on survival (not shown).

In summary, our study highlights the relevance of the peroxisomal FA catabolism machinery in metastatic spread, and we reveal CROT and CRAT as important players in melanoma progression and metastasis. Although these carnitine transferases have so far mainly been studied in the context of insulin resistance and cardiac metabolism, our study identifies acyl-carnitine shuttle as a potential therapeutic target in metastatic melanoma.

MATERIALS AND METHODS

Cell culture, survival, and FACS analysis

Cell lines (501mel, WM266-4, A375, WM9, WM98-1 [all *BRAF* sequence variant, and MV3 [*NRAS* mutated]) were grown in DMEM/25 mM glucose (Gibco, Madrid, Spain) with 10% fetal calf serum. For in vitro treatments (drugs and siRNA sequences are provided in Supplementary Materials and Methods), cells were cultured in suspension in DMEM/5 mM glucose for 72 hours before being replated; after 72 hours, they were analyzed using crystal violet as described (Aldaz et al., 2021). For FACS analysis, cells were cultured in adhesion or suspension in the presence of 25 or 5 mM glucose. At individual time points, cells were harvested, washed, and processed as described (Ferguson et al., 2017).

RNA sequencing and bioinformatics analysis

RNA was isolated from cells either grown in adherent or suspension conditions for 24 hours using an RNeasy Mini Kit (74104, Qiagen, Barcelona, Spain). The sequencing run was performed on an Illumina HiSeq1500, and data were processed as described (Aldaz et al., 2021). Ranked genes by log fold change were analyzed by gene set enrichment analysis using hallmark gene set (7.1) obtained from the Molecular Signatures Database (Liberzon et al., 2015) and the gene set enrichment analysis function ClusterProfiler (3.16.1) (Yu et al., 2012).

Experimental metastasis assays

After treatments (siRNA, drugs), viable 501mel cells stably expressing a luciferase/GFP reporter (Creusot et al., 2008) were injected into the tail vein of male *Rag2*$^{-/-}$; *Il2Rγ*$^{-/-}$ in-house bred mice (Rag2tm1.1FlvIl2rgtm1.1Flv/J, The Jackson Laboratory, Bar Harbor, ME, RRID:IMSR_JAX:014593). For imaging, mice were injected in the retro-orbital plexus with 50 μl of 15 mg/ml D-Luciferin, and photon flux was monitored using a PhotonIMAGER imaging system and analyzed using M3Vision software (Biospace Lab, Nesles-la-Vallée, France). All experiments in mice were performed in concordance with the Institutional Animal Care Committee of the University of Navarra (Pamplona, Spain) under protocols R-008c-18GN and R-057-18GN approved by the regional Government of Navarra in Spain.

qPCR and Western blotting

RNA extraction, quantitative RT-PCR, and western blotting followed standard protocols and were performed as described (Rowling et al., 2020; Sanz et al., 2000). Primary antibodies were cleaved caspase-3 (5A1E; number 9664, Cell Signaling Technologies, Boston, MA), extracellular signal–regulated kinase 2 (D-2; number sc-1647, Santa Cruz Biotechnology, Santa Cruz, CA), CROT (NBP1-85501), and CRAT (NBP1-86616, Novus Biologicals, Centennial, CO).

Data Analysis and Statistics

GraphPad Prism, version 7.00, for Mac operating system (GraphPad Software, San Diego, CA) was used for analysis. One-way ANOVA or Student's *t*-test was used for bar graph analyses, and log-rank test was used for Kaplan–Meier survival analyses. Data represent the results for assays performed from at least three replicates, and values are presented as the mean ± SEM. $^{*}P < 0.05$, $^{**}P < 0.01$, and $^{***}P < 0.001$.

Data availability statement

Datasets related to this article can be found at https://www.ncbi.nlm.nih.gov/geo/query/acc.cgi?acc=GSE208547 and have been deposited in the Gene Expression Omnibus database (www.ncbi.nlm.nih.gov/geo).

ORCIDs

Irene Lasheras-Otero: http://orcid.org/0000-0002-6806-3716
Iker Feliu: http://orcid.org/0000-0001-9279-3973
Alberto Maillo: http://orcid.org/0000-0002-3835-9794
Haritz Moreno: http://orcid.org/0000-0002-3640-8978
Marta Redondo-Muñoz: http://orcid.org/0000-0001-9726-7294
Paula Aldaz: http://orcid.org/0000-0003-3301-4866
Ana Bocanegra: http://orcid.org/0000-0002-3508-0595
Ana Olias-Arjona: http://orcid.org/0000-0001-6737-7089
Fernando Lecanda: http://orcid.org/0000-0002-7289-2293
Joaquin Fernandez-Irigoyen: http://orcid.org/0000-0001-5072-4099
Enrique Santamaria: http://orcid.org/0000-0001-8046-8102
Ignacio M. Larrayoz: http://orcid.org/0000-0003-1629-152X
David Gomez-Cabrero: http://orcid.org/0000-0003-4186-3788
Claudia Wellbrock: http://orcid.org/0000-0002-3825-6381
Silvestre Vicent: http://orcid.org/0000-0002-9457-6881
Imanol Arozarena: http://orcid.org/0000-0001-6349-2442

CONFLICT OF INTEREST

The authors state no conflict of interest.

ACKNOWLEDGMENTS

We thank Guadalupe Gutierrez and Beatriz Rodriguez from the Navarrabiomed Biobank for their help with the processing and staining of tumor samples. This work was funded by the Instituto de Salud Carlos III-FEDER through PI16-01911 and PI19/00645 to IA. IA and IML acknowledge support through Miguel Servet II fellowships (CPII20/00011 and CPII20/00029). The Health Department of the Government of Navarra, Spain funded work through reference GºNa 71/17. SV is funded by FEDER/Ministerio de Ciencia, Innovación y Universidades - Agencia Estatal de Investigación (PID2020-116344-RB-100) and by Foundation Spanish Association Against Cancer (PROYE20029VICE). ILO is funded through a Navarrabiomed PhD studentship and the Grupo Español Multidisciplinar de Melanoma (reference Beca_GEM). FL was funded by the Cancer Research Thematic Network of the Instituto de Salud Carlos III (RTICC RD12/0036/0066, SAF2015-71606R, RTI2018-094507-B-100) financed by MCIN/AEI/10.13039/501100011033 and by FEDER. FL was also funded by the la Caixa Foundation, Caja Navarra Foundation, and the Foundation AECC. PA is a recipient of a Sara Borrell postdoctoral fellowship from the Instituto de Salud Carlos III (CD21/00137).

AUTHOR CONTRIBUTIONS

Conceptualization: IA, SV, CW; Formal Analysis: AM, IML, DGC, JFI, ES, CW, SV, IA; Funding Acquisition: FL, SV, IA; Investigation: ILO, IF, HM, MRM, PA, AOA, AM, IML, DGC; Project Administration: IA; Supervision: IA, SV; Writing - Original Draft Preparation: IA, CW; Writing - Review and Editing: PA, FL, SV, CW, IA

SUPPLEMENTARY MATERIAL

Supplementary material is linked to the online version of the paper at www.jidonline.org, and at https://doi.org/10.1016/j.jid.2022.08.038

REFERENCES

Aldaz P, Auzmendi-Iriarte J, Durántez M, Lasheras-Otero I, Carrasco-Garcia E, Zelaya MV, et al. Identification of a dexamethasone mediated radioprotection mechanism reveals new therapeutic vulnerabilities in glioblastoma. Cancers (Basel) 2021;13:361.

Arozarena I, Wellbrock C. Targeting invasive properties of melanoma cells. FEBS Journal 2017;284:2148–62.

Arozarena I, Wellbrock C. Phenotype plasticity as enabler of melanoma progression and therapy resistance. Nat Rev Cancer 2019;19:377–91.

Bosc C, Broin N, Fanjul M, Saland E, Farge T, Courdy C, et al. Autophagy regulates fatty acid availability for oxidative phosphorylation through mitochondria-endoplasmic reticulum contact sites. Nat Commun 2020;11:4056.

Buchheit CL, Weigel KJ, Schafer ZT. Cancer cell survival during detachment from the ECM: multiple barriers to tumor progression. Nat Rev Cancer 2014;14:632–41.

Campbell NR, Rao A, Hunter MV, Sznurkowska MK, Briker L, Zhang M, et al. Cooperation between melanoma cell states promotes metastasis through heterotypic cluster formation. Dev Cell 2021;56:2808–25.e10.

Cancer Genome Atlas Network. Genomic classification of cutaneous melanoma. Cell 2015;161:1681–96.

Chapman A, Fernandez del Ama L, Ferguson J, Kamarashev J, Wellbrock C, Hurlstone A. Heterogeneous tumor subpopulations cooperate to drive invasion. Cell Rep 2014;8:688–95.

Creusot RJ, Yaghoubi SS, Kodama K, Dang DN, Dang VH, Breckpot K, et al. Tissue-targeted therapy of autoimmune diabetes using dendritic cells transduced to express IL-4 in NOD mice. Clin Immunol 2008;127:176–87.

Feinberg SM, Fariba KA, Saadabadi A. Thioridazine. Treasure Island, FL: StatPearls; 2022.

Ferguson J, Smith M, Zudaire I, Wellbrock C, Arozarena I. Glucose availability controls ATF4-mediated MITF suppression to drive melanoma cell growth. Oncotarget 2017;8:32946–59.

Fung C, Lock R, Gao S, Salas E, Debnath J. Induction of autophagy during extracellular matrix detachment promotes cell survival. Mol Biol Cell 2008;19:797–806.

Hernandez GA, Perera RM. Autophagy in cancer cell remodeling and quality control. Mol Cell 2022;82:1514–27.

Hoek KS, Schlegel NC, Brafford P, Sucker A, Ugurel S, Kumar R, et al. Metastatic potential of melanomas defined by specific gene expression profiles with no BRAF signature. Pigment Cell Res 2006;19:290–302.

Hong X, Roh W, Sullivan RJ, Wong KHK, Wittner BS, Guo H, et al. The lipogenic regulator SREBP2 induces transferrin in circulating melanoma cells and suppresses ferroptosis. Cancer Discov 2021;11:678–95.

Houten SM, Wanders RJA, Ranea-Robles P. Metabolic interactions between peroxisomes and mitochondria with a special focus on acylcarnitine metabolism. Biochim Biophys Acta Mol Basis Dis 2020;1866:165720.

Ju RJ, Stehbens SJ, Haass NK. The role of melanoma cell-stroma interaction in cell motility, invasion, and metastasis. Front Med (Lausanne) 2018;5:307.

Khoja L, Shenjere P, Hodgson C, Hodgetts J, Clack G, Hughes A, et al. Prevalence and heterogeneity of circulating tumour cells in metastatic cutaneous melanoma. Melanoma Res 2014;24:40–6.

Kongara S, Karantza V. The interplay between autophagy and ROS in tumorigenesis. Front Oncol 2012;2:171.

Konieczkowski DJ, Johannessen CM, Abudayyeh O, Kim JW, Cooper ZA, Piris A, et al. A melanoma cell state distinction influences sensitivity to MAPK pathway inhibitors. Cancer Discov 2014;4:816–27.

Le Gal K, Ibrahim MX, Wiel C, Sayin VI, Akula MK, Karlsson C, et al. Antioxidants can increase melanoma metastasis in mice. Sci Transl Med 2015;7:308re8.

Leighton F, Pérsico R, Necochea C. Peroxisomal fatty acid oxidation is selectively inhibited by phenothiazines in isolated hepatocytes. Biochem Biophys Res Commun 1984;120:505–11.

Liberzon A, Birger C, Thorvaldsdóttir H, Ghandi M, Mesirov JP, Tamayo P. The Molecular Signatures Database (MSigDB) hallmark gene set collection. Cell Syst 2015;1:417–25.

Luke JJ, Flaherty KT, Ribas A, Long GV. Targeted agents and immunotherapies: optimizing outcomes in melanoma. Nat Rev Clin Oncol 2017;14:463–82.

Luo C, Lim JH, Lee Y, Granter SR, Thomas A, Vazquez F, et al. A PGC1alpha-mediated transcriptional axis suppresses melanoma metastasis. Nature 2016;537:422–6.

McCormack JG, Stanley WC, Wolff AA. Ranolazine: a novel metabolic modulator for the treatment of angina. Gen Pharmacol 1998;30:639–45.

Micalizzi DS, Haber DA, Maheswaran S. Cancer metastasis through the prism of epithelial-to-mesenchymal transition in circulating tumor cells. Mol Oncol 2017;11:770–80.

Müller J, Krijgsman O, Tsoi J, Robert L, Hugo W, Song C, et al. Low MITF/AXL ratio predicts early resistance to multiple targeted drugs in melanoma. Nat Commun 2014;5:5712.

Muoio DM, Noland RC, Kovalik JP, Seiler SE, Davies MN, DeBalsi KL, et al. Muscle-specific deletion of carnitine acetyltransferase compromises glucose tolerance and metabolic flexibility. Cell Metab 2012;15:764–77.

Pascual G, Avgustinova A, Mejetta S, Martín M, Castellanos A, Attolini CS, et al. Targeting metastasis-initiating cells through the fatty acid receptor CD36. Nature 2017;541:41–5.

Piskounova E, Agathocleous M, Murphy MM, Hu Z, Huddlestun SE, Zhao Z, et al. Oxidative stress inhibits distant metastasis by human melanoma cells. Nature 2015;527:186–91.

Polioudaki H, Agelaki S, Chiotaki R, Politaki E, Mavroudis D, Matikas A, et al. Variable expression levels of keratin and vimentin reveal differential EMT status of circulating tumor cells and correlation with clinical characteristics and outcome of patients with metastatic breast cancer. BMC Cancer 2015;15:399.

Rowling EJ, Miskolczi Z, Nagaraju R, Wilcock DJ, Wang P, Telfer B, et al. Cooperative behaviour and phenotype plasticity evolve during melanoma progression. Pigment Cell Melanoma Res 2020;33:695–708.

Sanz V, Arozarena I, Crespo P. Distinct carboxy-termini confer divergent characteristics to the mitogen-activated protein kinase p38alpha and its splice isoform Mxi2. FEBS Lett 2000;474:169–74.

Schafer ZT, Grassian AR, Song L, Jiang Z, Gerhart-Hines Z, Irie HY, et al. Antioxidant and oncogene rescue of metabolic defects caused by loss of matrix attachment. Nature 2009;461:109–13.

Seiler SE, Martin OJ, Noland RC, Slentz DH, DeBalsi KL, Ilkayeva OR, et al. Obesity and lipid stress inhibit carnitine acetyltransferase activity. J Lipid Res 2014;55:635–44.

Shen S, Faouzi S, Souquere S, Roy S, Routier E, Libenciuc C, et al. Melanoma persister cells are tolerant to BRAF/MEK inhibitors via ACOX1-mediated fatty acid oxidation. Cell Rep 2020;33:108421.

Simpson CD, Anyiwe K, Schimmer AD. Anoikis resistance and tumor metastasis. Cancer Lett 2008;272:177–85.

Smith MP, Ferguson J, Arozarena I, Hayward R, Marais R, Chapman A, et al. Effect of SMURF2 targeting on susceptibility to MEK inhibitors in melanoma. J Natl Cancer Inst 2013;105:33–46.

Smith MP, Rowling EJ, Miskolczi Z, Ferguson J, Spoerri L, Haass NK, et al. Targeting endothelin receptor signalling overcomes heterogeneity driven therapy failure. EMBO Mol Med 2017;9:1011–29.

Tasdogan A, Ubellacker JM, Morrison SJ. Redox regulation in cancer cells during metastasis. Cancer Discov 2021;11:2682–92.

Trojaniello C, Luke JJ, Ascierto PA. Therapeutic advancements across clinical stages in melanoma, with a focus on targeted immunotherapy. Front Oncol 2021;11:670726.

Tsoi J, Robert L, Paraiso K, Galvan C, Sheu KM, Lay J, et al. Multi-stage differentiation defines melanoma subtypes with differential vulnerability to drug-induced iron-dependent oxidative stress. Cancer Cell 2018;33:890–904.e5.

Van den Branden C, Roels F. Thioridazine: a selective inhibitor of peroxisomal beta-oxidation in vivo. FEBS Lett 1985;187:331–3.

Vazquez F, Lim JH, Chim H, Bhalla K, Girnun G, Pierce K, et al. PGC1alpha expression defines a subset of human melanoma tumors with increased mitochondrial capacity and resistance to oxidative stress. Cancer Cell 2013;23:287–301.

Wang YN, Zeng ZL, Lu J, Wang Y, Liu ZX, He MM, et al. CPT1A-mediated fatty acid oxidation promotes colorectal cancer cell metastasis by inhibiting anoikis. Oncogene 2018;37:6025–40.

Watkins PA, Maiguel D, Jia Z, Pevsner J. Evidence for 26 distinct acyl-coenzyme A synthetase genes in the human genome. J Lipid Res 2007;48:2736–50.

Wolchok JD, Rollin L, Larkin J. Nivolumab and ipilimumab in advanced melanoma [published correction appears N Engl J Med 2018;379:2185] N Engl J Med 2017;377:2503–4.

Yu G, Wang LG, Han Y, He QY. clusterProfiler: an R package for comparing biological themes among gene clusters. Omics 2012;16:284–7.

SUPPLEMENTARY MATERIAL AND METHODS

Cell lines, culture, and reagents

The 501mel cells were a gift from Steve Rosenberg (National Cancer Institute, Bethesda, MD), WM266-4 (*BRAF* mutant) and A375 (*BRAF* mutant) cells were bought from ATCC (Manassas, VA), WM9 (*BRAF* mutant), and WM98-1 (*BRAF* mutant) and MV3 (*NRAS* mutant) cells were a gift from Adam Hurlstone (University of Manchester, Manchester, United Kingdom). All cell lines have been authenticated in 2021. To culture cells in suspension, six-well plates were coated with 1 ml of a sterile solution of 2% agar in water. Once the agar had solidified, half a million cells (125,000 cells/ml) in DMEM, 1% fetal calf serum, and 5 mM glucose were plated per well and cultured for up to 3 days. Treatments lasting 72 hours were initiated 5 hours after plating. At the end of any treatment, cells were collected in 15 ml tubes, spun for 5 minutes at 1,500 r.p.m., and then subjected to the respective method of analysis. For all experiments, cells defrosted from a single vial were used for no more than 1 month or six passages. Thioridazine (T9025, Sigma-Aldrich, St Louis, MO), ranolazine, Z-VAD-FMK, liproxstatin-1, and ferrostatin-1 (HY-17401, HY-16658B, HY-12726, and HY-100579, MedChemExpress, Gijon, Spain), octanoic and decanoic acid (W279900 and W236403, Merck, Madrid, Spain) were reconstituted in DMSO.

Mice

We used *Rag2*$^{-/-}$; *Il2R*$\gamma^{-/-}$ in-house bred mice (Rag2tm1.1Flv|l2rgtm1.1Flv/J, The Jackson Laboratories, Bar Harbor, ME, RRID:IMSR_JAX:014593). All experiments in mice were performed following Animal Research: Reporting of In Vivo Experiments guidelines and in concordance with the Institutional Animal Care Committee of the University of Navarra (Pamplona, Spain) under the protocol numbers R-008c-18GN and R-057-18GN approved by the regional Government of Navarra in Spain. After injection into the tail vein, mice were randomized by age. After imaging, photon flux was calculated for each mouse using a region of interest at the indicated times for 4 weeks. On day 28, mice were killed, and after D-luciferin injection, ex vivo bioluminescence intensity was measured.

qRT-PCR and primers

For qRT-PCR experiments, total RNA was extracted and analyzed as described previously (Aldaz et al., 2021). Primer sequences were as follows: ABCD1 forward, 5′-CACCCCAGCGCATGTTCTAC and ABCD1 reverse, 5′-ACACATAGCCTCCCAACCTCC; ABCD3 forward, 5′-ACGGGTATTTCATGGAAACTTGGA and ABCD3 reverse, 5′-GCTCCTTTTTCCCCTCTTTCTCA; ACAA2 forward, 5′-CATCGGGTGTAGCTGATGGT and ACAA2 reverse, 5′-AGCAGGGACAGGACCAATAC; ACOX1 forward, 5′-GGTTTAAAAATTTTGTGCACCGAGG and ACOX1 reverse, 5′-CGAAGGTGAGTTCCATGACCC; CPT1A forward, 5′-GACGTGGGAAAAATAAGCAGTC and CPT1A reverse, 5′-ACATCGGCCGTGTAGTAGAGAT; CPT1C forward, 5′-CAGTTGGCTTTTCCTCTTCAGT and CPT1C reverse, 5′-AGGCAGCAACTCTTTGATCTTC; CPT2 forward, 5′-AAAGAAGCAGCAATGGGCCAG and CPT2 reverse, 5′-ATGCAGGGTCCAGGTAGAGC; CRAT forward, 5′-GGAAGACGGAGAACTGGCTG and CRAT reverse, 5′-TGAGTTTGGCAGCAAATCGGA; CROT forward, 5′-CGCCAGAGCTTCTCAGACAAC and CROT reverse, 5′-CCTTAGCCCATCGAGTTCGC; EHHADH forward, 5′-ATAGGATTGCCCACGCAGAG and EHHADH reverse, 5′-TGCTAAAATACGTCTTCCTGAGGT; ETFB forward, 5′-TCCTGCTGGGCAGATCCGA and ETFB reverse, 5′-CGGTACGAATCGTCTCCTGGC; and SLC25A20 forward, 5′-CGACCAGCCAAAACCCATCA and SLC25A20 reverse, 5′-GTGTCTGCAGTCGGACCTTG.

RNA interference and small interfering RNA sequences

For RNA interference experiments, cells were transfected with small interfering RNAs (siRNAs) using Lipofectamine Transfection Reagent (18324020, Thermo Fisher Scientific, Loughborough, United Kingdom) in adherent conditions. Forty-eight hours later, cells were counted and cultured in suspension for 72 hours. Then, cells were replated and analyzed after 72 hours as described (Aldaz et al., 2021). Human ON-TARGETplus SMARTpools (Horizon Discovery, Waterbeach, United Kingdom) used were ABCD1-targeted siRNA (number L-009605-00), ABCD3-targeted siRNA (number L-009909-00), ACOX1-targeted siRNA (number L-005074-00), CPT1A-targeted siRNA (number L-009749-00), CRAT-targeted siRNA (number L-009524-00), CROT-targeted siRNA (number L-009230-00), EHHADH-targeted siRNA (number L-009822-00), ETFB-targeted siRNA (number L-010494-00), and SLC25A20-targeted siRNA (number L-007480-00). Sequences for individual small interfering RNAs were scrambled control, AAACCGUCGAUUUCACCCGGGUU; siRNA targeting SLC25A20#6, GAAAGCAAGUACACUGGUA; siRNA targeting SLC25A20#7, GAUGUUAUCUGGCGUAUUC; siRNA targeting SLC25A20#8, GCCAUGAAGUUCCUUAAUU; siRNA targeting SLC25A20#9, CAACUGGGCUGUGGCAAUC; siRNA targeting CROT#6, GUAUAACUCUUUGGCAUAA; siRNA targeting CROT#7, GAACUACUGGCAGCUAUUA; siRNA targeting CROT#9, GUAGUUUACUGGUAUAUUC; siRNA targeting CRAT#6, ACUCAUCCCUACAGACCAA; siRNA targeting CRAT#7, GUACCACAGUGACGGGACA; and siRNA targeting CRAT#8, CCAAGAAGCUGCGGUUCAA.

SUPPLEMENTARY REFERENCES

Aldaz P, Auzmendi-Iriarte J, Durántez M, Lasheras-Otero I, Carrasco-Garcia E, Zelaya MV, et al. Identification of a dexamethasone mediated radioprotection mechanism reveals new therapeutic vulnerabilities in glioblastoma. Cancers (Basel) 2021;13:361.

Liberzon A, Birger C, Thorvaldsdóttir H, Ghandi M, Mesirov JP, Tamayo P. The Molecular Signatures Database (MSigDB) hallmark gene set collection. Cell Syst 2015;1:417–25.

Supplementary Figure S1. Cell-autonomous characteristics in nonadherent melanoma cells. (**a**) Cell cycle profiles of 501mel and WM266-4 cells grown in ADH or SUSP as indicated. (**b**) Principal component analysis of 501mel and WM266-4 cells cultured in ADH or SUSP in the presence of 25 or 5 mM glucose for 24 hours. (**c**) Cluster analysis of the transcriptomic profile of WM266-4 cells cultured as indicated. (**d**) GSEA plots for MSigDB hallmarks (Liberzon et al., 2015) significantly different in 501mel SUSP cells from that in ADH cells grown in the presence of 25 mM glucose. ADH, adhesion; GSEA, gene set enrichment analysis; h, hour; MSigDB, Molecular Signatures Database; PC, principal componenet; SUSP, suspension.

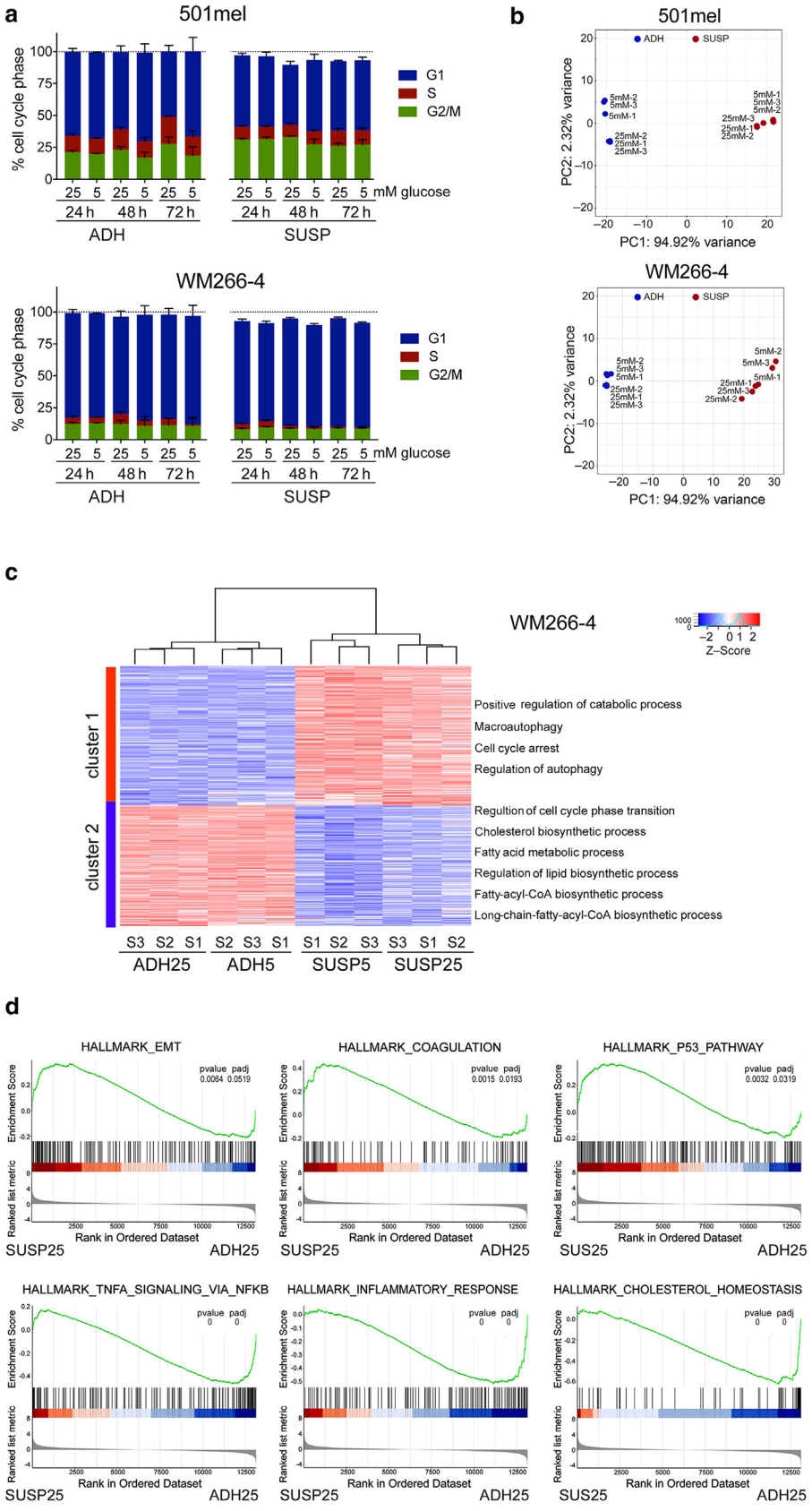

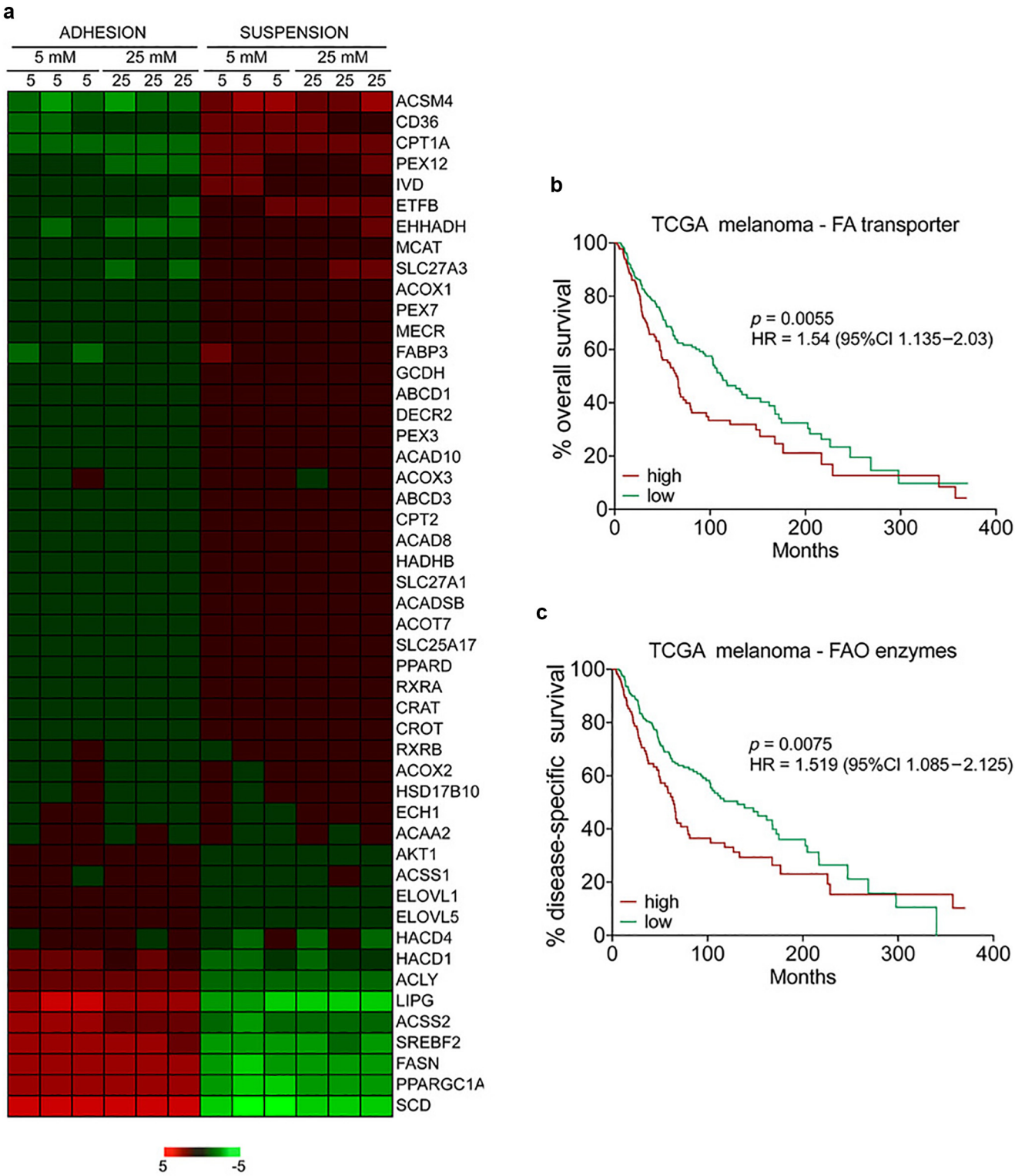

Supplementary Figure S2. FAO regulator upregulation correlates with poorer survival. (**a**) Heatmap of upregulated and downregulated genes in WM266-4 cells cultured as indicated. (**b, c**) Kaplan–Meier analysis of the TCGA melanoma patient cohort (Cancer Genome Atlas Network, 2015). Differences in survival for patients whose tumors express high or low levels of (**b**) CPT1C, SLC25A20, CPT2, CPT1A, SLC27A1, SLC27A3, and CD36 or of (**c**) CROT, CRAT, ACACB, ACAA2, ECH1, ACADS, ACOT7, ACOT9, ECHS1, and HSD17B10 are shown. Respective genes were analyzed for mRNA expression (z-score = 2.0) in cBioportal, and survival data were extracted and analyzed in GraphPad Prism. CI, confidene interval; CRAT, carnitine acetyltransferase; CROT, carnitine O-octanoyltransferase; FA, fatty acid; FAO, fatty acid beta-oxidation; HR, hazard ratio; TCGA, The Cancer Genome Atlas.

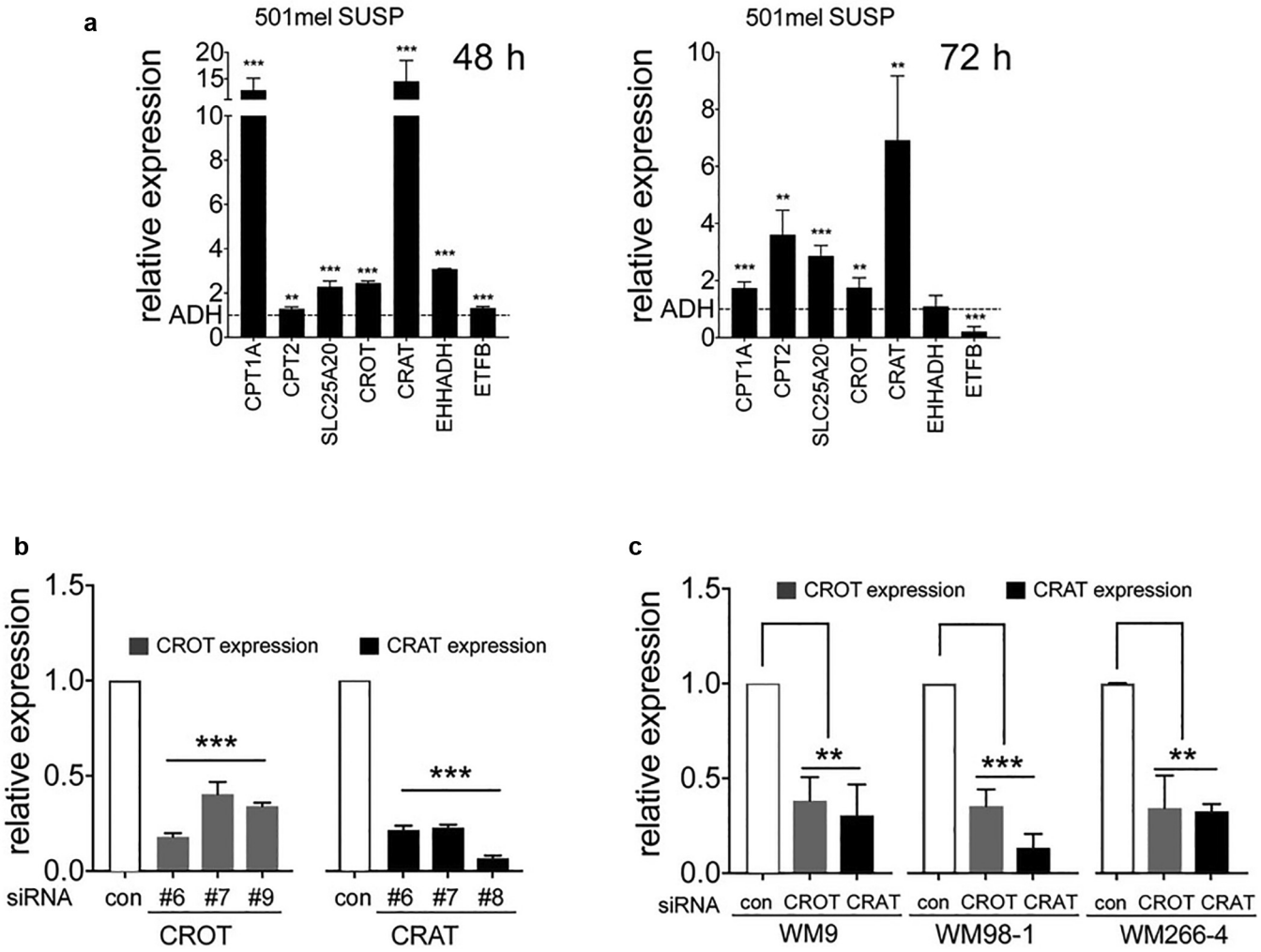

Supplementary Figure S3. CROT and CRAT in melanoma cells. (**a**) qRT-PCR analysis of the indicated genes in 501mel cells grown in suspension for 48 or 72 hours. The expression of cells grown in adhesion was set to 1. (**b**) qRT-PCR analysis for CROT or CRAT expression in 501mel cells 48 hours after CROT or CRAT RNAi. Expression in cells treated with control siRNA was set 1. (**c**) qRT-PCR analysis for CROT or CRAT expression in the indicated cell lines after CROT or CRAT RNAi. ADH, adhesion; con, control; CRAT, carnitine acetyltransferase; CROT, carnitine O-octanoyltransferase; h, hour; RNAi, RNA interference; siRNA, small interfering RNA; SUSP, suspension.

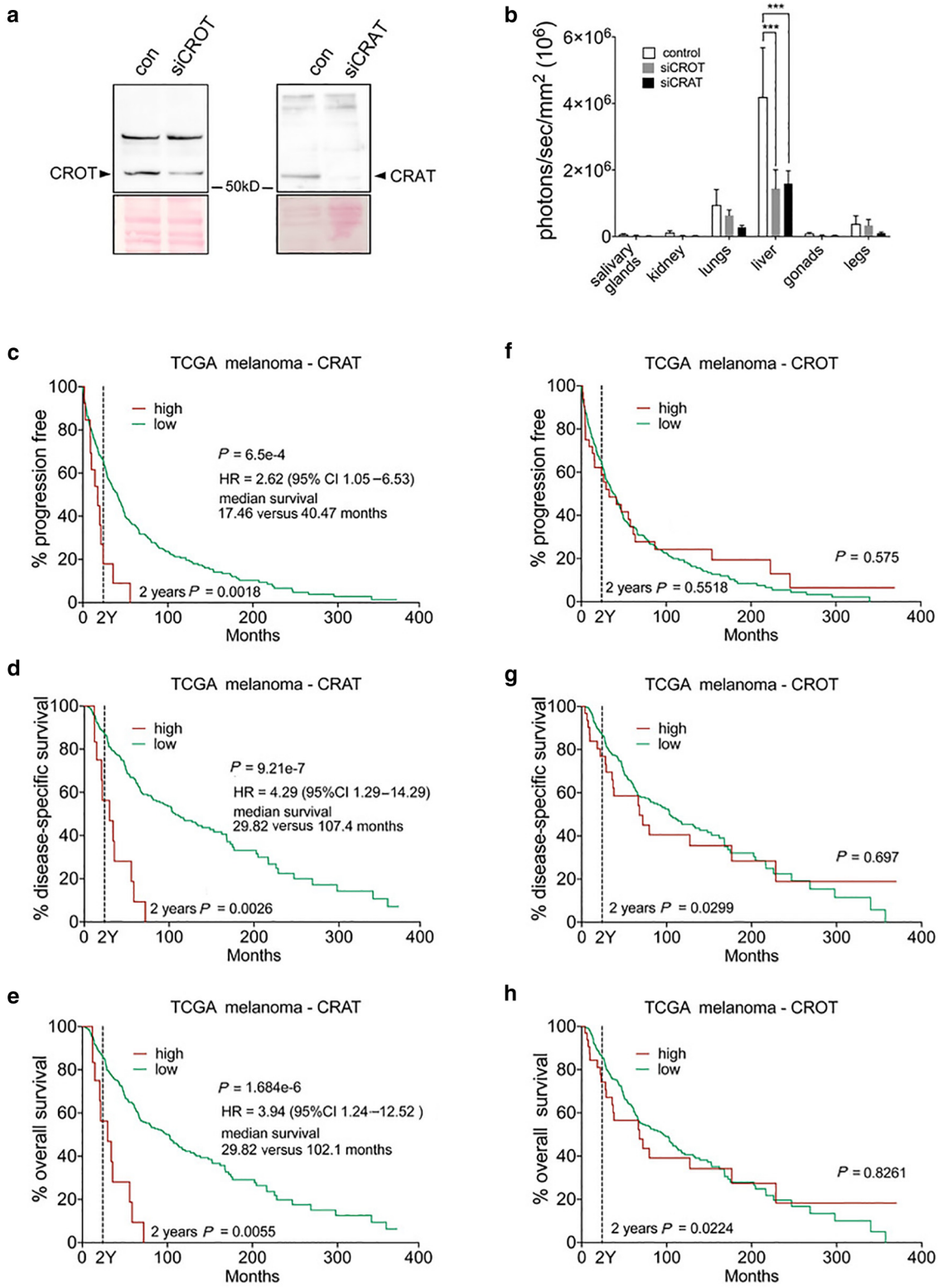

Supplementary Figure S4. CROT and CRAT correlation with melanoma metastasis, progression, and survival. This figure is related to Figure 4. (**a**) Western blot for CROT and CRAT 66 hours after RNAi in 501mel-GFP cells. (**b**) Ex vivo bioluminescence quantification of 501mel tumor burden in the indicated organs. Graphs show the mean ± SEM signal of organs from six (control, CRAT) or five (CROT) mice. $^{**}P < 0.01$ and $^{***}P < 0.001$ with one-way ANOVA. (**c–h**) Kaplan–Meier analyses of the TCGA melanoma patient cohort (Cancer Genome Atlas, 2015) for (**c, f**) progression-free, (**d, g**) disease-specific, and (**e, h**) overall survival of patients whose tumors express high or low levels of CRAT or CROT, respectively. Respective genes were analyzed in cBioportal, and survival data were extracted and analyzed in GraphPad Prism. CI, confidence interval; con, control; CRAT, carnitine acetyltransferase; CROT, carnitine O-octanoyltransferase; HR, hazard ratio; RNAi, RNA interference; siCRAT, carnitine acetyltransferase–targeted small interfering RNA; siCROT, carnitine O-octanoyltransferase–targeted small interfering RNA; TCGA, The Cancer Genome Atlas.